Cable equation for general geometry

Erick J. López-Sánchez[*]
Posgrado en Ciencias Naturales e Ingeniería, Universidad Autónoma Metropolitana, Cuajimalpa and Vasco de Quiroga 4871, Santa Fe Cuajimalpa, Ciudad de México 05300, México

Juan M. Romero[†]
Departamento de Matemáticas Aplicadas y Sistemas, Universidad Autónoma Metropolitana-Cuajimalpa, Vasco de Quiroga 4871, Santa Fe Cuajimalpa, Ciudad de México 05300, México

(Received 30 June 2016; revised manuscript received 2 December 2016; published 13 February 2017)

The cable equation describes the voltage in a straight cylindrical cable, and this model has been employed to model electrical potential in dendrites and axons. However, sometimes this equation might give incorrect predictions for some realistic geometries, in particular when the radius of the cable changes significantly. Cables with a nonconstant radius are important for some phenomena, for example, discrete swellings along the axons appear in neurodegenerative diseases such as Alzheimers, Parkinsons, human immunodeficiency virus associated dementia, and multiple sclerosis. In this paper, using the Frenet-Serret frame, we propose a generalized cable equation for a general cable geometry. This generalized equation depends on geometric quantities such as the curvature and torsion of the cable. We show that when the cable has a constant circular cross section, the first fundamental form of the cable can be simplified and the generalized cable equation depends on neither the curvature nor the torsion of the cable. Additionally, we find an exact solution for an ideal cable which has a particular variable circular cross section and zero curvature. For this case we show that when the cross section of the cable increases the voltage decreases. Inspired by this ideal case, we rewrite the generalized cable equation as a diffusion equation with a source term generated by the cable geometry. This source term depends on the cable cross-sectional area and its derivates. In addition, we study different cables with swelling and provide their numerical solutions. The numerical solutions show that when the cross section of the cable has abrupt changes, its voltage is smaller than the voltage in the cylindrical cable. Furthermore, these numerical solutions show that the voltage can be affected by geometrical inhomogeneities on the cable.

DOI: 10.1103/PhysRevE.95.022403

I. INTRODUCTION

Understanding how the brain works is relevant for different medical and technological applications. In this respect it is central to know the electrical brain activity. The basic unit in the brain is the neuron, which transmits electrical signals through axons and receives electrical signals through dendrites. Thus, it is important to understand the electrical behavior of dendrites and axons. Axons and dendrites can be described as cables with special properties. It is worth mentioning that the first model for an electrical cable was proposed by Lord Kelvin in the telegraph problem context. Inspired by the Lord Kelvin's work, different authors have proposed models to describe dendrites and axons. For example, Rall proposed that a dendrite can be taken as a cable with a circular cross section and constant diameter d_0 where the voltage $V(x,t)$ satisfies the cable equation [1–4]

$$c_M \frac{\partial V(x,t)}{\partial t} = \frac{d_0}{4r_L} \frac{\partial^2 V(x,t)}{\partial x^2} - i_{\text{ion}}, \tag{1}$$

where c_M denotes the specific membrane capacitance, r_L denotes the longitudinal resistance, and i_{ion} is the ionic current per unit area into and out of the cable. In the passive cable case, namely when $i_{\text{ion}} = V/r_M$, with r_M the specific membrane resistance, Eq. (1) is exactly solved [3–5].

The cable equation has been useful to explain different phenomena in dendrites and axons [3–5]. However, there are axons and dendrites with different geometry, in particular axons and dendrites with a variable radius, and the cable equation only describes cylindrical cables with a constant radius. Furthermore, there are phenomena where the geometry of the axons and dendrites is relevant. For example, axons with a nonconstant radius are hallmark features of some neurodegenerative diseases. Actually, discrete swellings along the axons appear in neurodegenerative diseases such as Alzheimers, Parkinsons, human immunodeficiency virus (HIV)-associated dementia, and multiple sclerosis [6–8]. Remarkably, in extreme cases, the electrical signal is deleted in the swelling of the axon. Additionally, theoretical and experimental studies show that dendritic geometry determines the efficacy of voltage propagation [9,10]. Another example of dendrites with nontrivial geometry is given by spiny dendrites which exhibit anomalous diffusion [11]. In addition, dendrites with varying diameter are found in synaptic contacts, retina amacrine cells, the cerebellar dentate nucleus, and the lateral vestibular nucleus, as well as cortical pyramidal and olfactory bulb cells [12–14]. Furthermore, recent theoretical studies emphasize the spatial variability of dendritic calcium dynamics due to local changes in a dendrite diameter [15]. For these reasons, it is important to study cables with general geometry. Some extensions of the cable model can be seen in Refs. [16–18].

In this paper, using the Frenet-Serret frame, we propose a cable with general geometry and construct a generalized

[*]lsej@unam.mx
[†]jromero@correo.cua.uam.mx

cable equation for the voltage in it. This generalized equation depends on geometric quantities as curvature and torsion of the cable. For the general case, this new equation is very complicated. Nevertheless, we show that when the cable has a constant circular cross section the generalized cable equation depends on neither the curvature nor the torsion of the cable. In fact, in this last case the new cable equation is equivalent to the cable equation for a straight cylindrical cable. Moreover, we find an exact solution for an ideal cable with a particular variable circular cross section and zero curvature. In this case, we show that when radius increases the voltage decreases. Inspired in this ideal case, we rewrite the generalized cable equation as a diffusion equation with a source term. In this diffusion equation the source term and the diffusion coefficient are generated by the cable geometry. In addition, we provide numerical solutions to different cable with swelling. The numerical solutions show that when the radius of the cable has notable changes its voltage is smaller than the voltage in the cylindrical cable. Furthermore, the numerical solutions show that the voltage can be affected by geometrical inhomogeneities on the cable. These numerical results are consistent with the behavior of the voltage in focal axonal swellings [6].

This paper is organized as follows: In Sec. II we propose a cable with a general geometry; in Sec. III we propose a generalized cable equation; in Sec. IV we study a cable with a circular cross section; in Sec. V we study a particular cable with a variable radius; in Sec. VI we study some general properties of the generalized cable equation; and, in Sec. VII, we provide numerical solutions to the cable equation. Finally, in Sec. VIII a summary is given.

II. CABLE GEOMETRY

It is well known that a three-dimensional curve $\vec{\gamma}$ can be reparametrized with different parameters and its geometric properties are invariant under reparametrizations. For example, the arc length of the curve $\vec{\gamma}$ is given by

$$s = \int_0^x \sqrt{\frac{d\vec{\gamma}(\zeta)}{d\zeta}\frac{d\vec{\gamma}(\zeta)}{d\zeta}}\,d\zeta, \tag{2}$$

which is invariant under reparametrization on ζ. Notably, the arc length parameter (2) is a friendly parameter to study the geometric properties of a tridimensional curve. For instance, using the arc length parameter (2) we can construct the vectors of the Frenet-Serret frame [19]

$$\frac{d\vec{\gamma}(s)}{ds} = \hat{T}, \quad \hat{N} = \frac{\frac{d\hat{T}}{ds}}{\left|\frac{d\hat{T}}{ds}\right|}, \quad \hat{B} = \hat{T}\times\hat{N}, \tag{3}$$

where $\hat{T}$ is the unit vector tangent, $\hat{N}$ is the normal unit vector, and $\hat{B}$ is the binormal unit vector to the curve.

Furthermore, using the arc length and the Frenet-Serret frame, the Frenet-Serret formulas can be obtained as follows [19]:

$$\frac{d\hat{T}}{ds} = \kappa\hat{N}, \quad \frac{d\hat{N}}{ds} = -\kappa\hat{T} + \tau\hat{B}, \quad \frac{d\hat{B}}{ds} = -\tau\hat{N}, \tag{4}$$

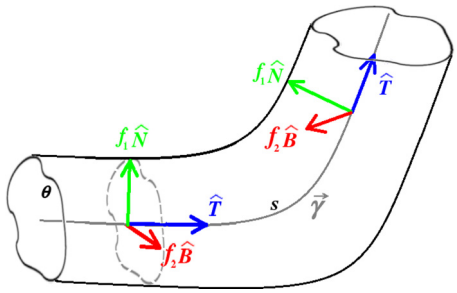

FIG. 1. Cable with general geometry. The vectors $\hat{T},\hat{N},\hat{B}$ are shown in two different points on the curve $\vec{\gamma}$

where κ and τ are the curvature and torsion of the curve $\vec{\gamma}$, respectively.

We can employ the Frenet-Serret frame to construct a cable model. Actually, we can propose a general cable as the region bounded by the following surface:

$$\vec{\Sigma}(\theta,s) = \vec{\gamma}(s) + f_1(\theta,s)\hat{N}(s) + f_2(\theta,s)\hat{B}(s), \tag{5}$$

where θ is an angular variable. Notice that employing the angular coordinate θ, the functions $f_1(\theta,s), f_2(\theta,s)$, and the vectors $\hat{N}(s), \hat{B}(s)$, we are constructing the cable over the curve $\vec{\gamma}(s)$. For example, a cable with a circular cross section with radius $R(s)$ can be parameterized with the functions

$$f_1(\theta,s) = R(s)\cos\theta, \quad f_2(\theta,s) = R(s)\sin\theta. \tag{6}$$

In Fig. 1 we can see a representation of the surface (5).

Some geometric quantities as the area of a surface can be written in terms of the first fundamental form, which is constructed with the inner product on the tangent space of a surface [19]. In the case of the surface (5) we have

$$g = \begin{pmatrix} E & F \\ F & G \end{pmatrix}, \tag{7}$$

where the first form coefficients are

$$E = \left|\frac{\partial\vec{\Sigma}(\theta,s)}{\partial s}\right|^2 = (1-\kappa f_1)^2 + \left(\frac{\partial f_1}{\partial s} - \tau f_2\right)^2 + \left(\frac{\partial f_2}{\partial s} + \tau f_1\right)^2, \tag{8}$$

$$G = \left|\frac{\partial\vec{\Sigma}(\theta,s)}{\partial\theta}\right|^2 = \left(\frac{\partial f_1}{\partial\theta}\right)^2 + \left(\frac{\partial f_2}{\partial\theta}\right)^2, \tag{9}$$

$$F = \frac{\partial\vec{\Sigma}(\theta,s)}{\partial s}\cdot\frac{\partial\vec{\Sigma}(s,\theta)}{\partial\theta} = \left(\frac{\partial f_1}{\partial s} - \tau f_2\right)\frac{\partial f_1}{\partial\theta} + \left(\frac{\partial f_2}{\partial s} + \tau f_1\right)\frac{\partial f_2}{\partial\theta}. \tag{10}$$

Using the first fundamental form, an area element of the cable surface (5) can be written as

$$\Delta A = \left[\int_0^{2\pi} d\theta\sqrt{\det g(\theta,s)}\right]\Delta s, \tag{11}$$

where

$$\det g(\theta,s) = \left[\left(\frac{\partial f_1}{\partial s}\frac{\partial f_2}{\partial \theta} - \frac{\partial f_2}{\partial s}\frac{\partial f_1}{\partial \theta}\right) - \frac{\tau}{2}\frac{\partial}{\partial \theta}\left(f_1^2 + f_2^2\right)\right]^2 + (1-\kappa f_1)^2\left[\left(\frac{\partial f_1}{\partial \theta}\right)^2 + \left(\frac{\partial f_2}{\partial \theta}\right)^2\right]. \tag{12}$$

Notice that the area element (11) depends on the curvature κ and the torsion τ of the curve $\vec{\gamma}$.

In particular, when the cable has a circular cross section with radius $R(s)$, namely when the cable is reparametrized with the functions (6), the area element of cable surface (5) is given by

$$\Delta A = R(s)\Delta s \int_0^{2\pi} d\theta \sqrt{(1-\kappa(s)R(s)\cos\theta)^2 + \left[\frac{dR(s)}{ds}\right]^2}, \tag{13}$$

while the cable cross-sectional area is

$$a(s) = \pi R^2(s). \tag{14}$$

We can see that the area element (13) does not depend on the torsion τ of the curve $\vec{\gamma}$.

Now, the Gaussian curvature characterizes the curvature of a surface [19]. In particular, if the cable (5) has a circular cross section with a constant radius R_0, then the Gaussian curvature of the surface of this cable is given by

$$K = -\frac{\kappa(s)\cos\theta}{R_0[1-\kappa(s)R_0\cos\theta]}. \tag{15}$$

Notice that this quantity is singular when $\kappa(s)R_0 \geqslant 1$. Because of the surfaces of the axons or dendrites reported are smooth surfaces, we can suppose that the Gaussian curvature of the surfaces of axons or dendrites does not have singularities. Notice that this hypothesis implies the inequality $\kappa(s)R_0 < 1$. In addition, let us remember that the curvature $\kappa(s)$ at a point P of the curve $\vec{\gamma}(s)$ is defined as the inverse of the radius of the osculating circle at P, see Ref. [20]. Then, if at this point P the cable radius is $R(s)$, then the radius of the osculating circle must be larger than $R(s)$. Thus, at the point P the curvature $\kappa(s)$ must be smaller than $R^{-1}(s)$ and the following inequality:

$$\kappa(s)R(s) < 1 \tag{16}$$

is satisfied. In this paper we suppose that the inequality (16) is always satisfied.

Furthermore, notice that when $R(s) = R_0 = \text{const}$ the area element (13) is given by

$$\Delta A = 2\pi R_0 \Delta s \tag{17}$$

and it depends on neither the torsion τ nor the curvature κ.

In the next section we will propose a cable equation when a cable is described by (5).

III. CABLE EQUATION

In order to propose a cable equation to a cable with the geometry given by the equation (5), we break the curve $\vec{\gamma}(s)$ into n pieces. Each piece has a surface area ΔA_i and a cross-sectional area a_i $(i = 0,1,2\cdots n)$.

Now, we consider a current flow I_{long} along the cable. Then, if $V(s,t)$ is the membrane potential and R_L is the resistance of the cable, from the Ohm's law, then we have

$$V(s+\Delta s,t) - V(s,t) = -I_{\text{long}}(s,t)R_L. \tag{18}$$

In addition, due to the fact that the resistance to a cable with a cross-sectional area $a(s)$ is [21],

$$R_L = \frac{r_L \Delta s}{a(s)}, \tag{19}$$

where r_L is the specific intracellular resistivity, from the Ohm's law (18) we obtain

$$I_{\text{long}} = -\frac{a(s)}{r_L}\left[\frac{V(s+\Delta s,t) - V(s,t)}{\Delta s}\right] \approx -\frac{a(s)}{r_L}\frac{\partial V(s,t)}{\partial s}. \tag{20}$$

Furthermore, if C_M is the membrane capacitance, then we get

$$Q_{\text{cap}} = VC_M, \tag{21}$$

which implies

$$I_{\text{cap}} = \frac{dQ}{dt} = C_M\frac{\partial V(s,t)}{\partial t}. \tag{22}$$

Observe that the capacitance for the cable surface can be taken as

$$C_M = \Delta A(s)c_M, \tag{23}$$

where c_M is the specific membrane capacitance. Thus, the equation (22) can be written as

$$I_{\text{cap}} = \Delta A(s)c_M\frac{\partial V(s,t)}{\partial t}. \tag{24}$$

Moreover, the total ionic current that flows across the membrane is

$$I_{\text{ion}} = (\Delta A)i_{\text{ion}}, \tag{25}$$

where i_{ion} is the current per unit area into and out of the cable.

Hence, the change in cable current is given by

$$I_{\text{cap}} + I_{\text{ion}} = -I_{\text{long}}(s+\Delta s,t) + I_{\text{long}}(s,t), \tag{26}$$

which implies

$$\Delta A(s)c_M\frac{\partial V(s,t)}{\partial t} + (\Delta A)i_{\text{ion}} \approx \frac{a(s+\Delta s)}{r_L}\frac{\partial V(s+\Delta s,t)}{\partial s} - \frac{a(s)}{r_L}\frac{\partial V(s,t)}{\partial s},$$

and then

$$\frac{\partial V(s,t)}{\partial t} + \frac{i_{\text{ion}}}{c_M} \approx \frac{a(s+\Delta s)\frac{\partial V(s+\Delta s,t)}{\partial s} - a(s)\frac{\partial V(s,t)}{\partial s}}{r_L\Delta A(s)c_M}. \tag{27}$$

Because the cable surface area is given by Eq. (11), we obtain

$$\frac{\partial V(s,t)}{\partial t} + \frac{i_{\text{ion}}}{c_M} \approx \frac{1}{r_L c_M \int du\sqrt{\det g(u,s)}} \times \left[\frac{a(s+\Delta s)\frac{\partial V(s+\Delta s,t)}{\partial s} - a(s)\frac{\partial V(s,t)}{\partial s}}{\Delta s}\right].$$

Thus, at the limit $\Delta s \to 0$, we arrive at

$$\frac{\partial V(s,t)}{\partial t} = \frac{1}{r_L c_M \int_0^{2\pi} d\theta \sqrt{\det g(\theta,s)}} \frac{\partial}{\partial s}\left[a(s)\frac{\partial V(s,t)}{\partial s}\right] - \frac{i_{\text{ion}}}{c_M}. \tag{28}$$

This equation is the cable equation when the cable geometry is given by (5) and it depends on geometric quantities as the curvature κ and torsion τ of the cable.

In the general case, i_{ion} depends on the voltage and Eq. (28) is a nonlinear differential equation. However, in the passive cable model we can take

$$i_{\text{ion}} = \frac{V(s,t)}{r_M}. \tag{29}$$

Therefore, the cable equation for the passive cable model with the geometry given by (5) is

$$\frac{\partial V(s,t)}{\partial t} = \frac{1}{r_L c_M \int_0^{2\pi} d\theta \sqrt{\det g(\theta,s)}} \frac{\partial}{\partial s}\left[a(s)\frac{\partial V(s,t)}{\partial s}\right] - \frac{V(s,t)}{r_M c_M}. \tag{30}$$

For an infinite cable, the voltage has to satisfy the Dirichlet boundary condition, while for a finite cable the voltage has to satisfy the Neumann boundary condition [3].

In the next section we will study some exactly solvable cases of Eq. (30).

IV. CIRCULAR CROSS SECTION

A cable with a deformed circular cross section where the radius depends on the angle θ, namely $R = R(\theta,s)$, can be modeled with the surface (5), where

$$f_1(\theta,s) = R(\theta,s)\cos\theta, \quad f_2(\theta,s) = R(\theta,s)\sin\theta. \tag{31}$$

In this case the cross-sectional area is given by

$$a(s) = \frac{1}{2}\int_0^{2\pi} R^2(\theta,s)d\theta, \tag{32}$$

in addition we obtain

$$\sqrt{\det g(\theta,s)} = \left(R^2(\theta,s)\left[\frac{\partial R(\theta,s)}{\partial s} - \tau\frac{\partial R(\theta,s)}{\partial \theta}\right]^2 + (1-\kappa(s)R(\theta,s)\cos\theta)^2 \times \left\{R^2(\theta,s) + \left[\frac{\partial R(\theta,s)}{\partial \theta}\right]^2\right\}\right)^{\frac{1}{2}}. \tag{33}$$

For this general cable geometry, to find solutions of the cable equation (30) is a difficult task. However, for some cases this equation can be simplified. For instance, when the cable has a circular cross section, namely when $R(\theta,s) = R(s)$, the function (33) does not depend on the torsion of the cable τ. Hence, in this case the cable equation (30) becomes

$$\frac{\partial V(s,t)}{\partial t} = \frac{\pi \frac{\partial}{\partial s}\left[R^2(s)\frac{\partial V(s,t)}{\partial s}\right]}{r_L c_M R(s)\int_0^{2\pi} d\theta \sqrt{(1-\kappa(s)R(s)\cos\theta)^2 + \left[\frac{dR(s)}{ds}\right]^2}} - \frac{V(s,t)}{r_M c_M}. \tag{34}$$

Notice that if the sectional area is constant, that is, $R(s) = R_0 = \text{const}$, Eq. (34) is given by

$$\frac{\partial V(s,t)}{\partial t} = \frac{R_0}{2c_M r_L}\frac{\partial^2 V(s,t)}{\partial s^2} - \frac{V(s,t)}{r_M c_M}. \tag{35}$$

Remarkably, this last equation depends on neither the curvature nor the torsion of the cable. Furthermore, Eq. (35) is equivalent to the cable equation for a straight cylindrical cable (1). Observe that Eq. (35) depends on the arc length parameter (2) instead of the laboratory frame coordinate x. This shows that the natural variables for the voltage are given by geometric quantities of the cable.

For an infinite cable, the solution of Eq. (35) is

$$V(s,t) = V_0 l_0 \sqrt{\frac{r_L c_M}{2\pi R_0 t}} e^{-\frac{r_L c_M s^2}{2R_0 t}} e^{-\frac{t}{r_M c_M}}, \tag{36}$$

where V_0 is a constant with voltage dimensions and l_0 is a constant with length dimensions. Notice that in this case the initial condition

$$V(s,0) = V_0 l_0 \delta(s) \tag{37}$$

is satisfied, where $\delta(s)$ is the Dirac δ function. Moreover, using the laboratory frame coordinate x and Eq. (2), the voltage (36) can be written as

$$V(x,t) = V_0 l_0 \sqrt{\frac{r_L c_M}{2\pi R_0 t}} e^{-\frac{r_L c_M \left[\int_0^x \sqrt{\frac{d\vec{\gamma}(\zeta)}{d\zeta}\cdot\frac{d\vec{\gamma}(\zeta)}{d\zeta}}\, d\zeta\right]^2}{2R_0 t}} e^{-\frac{t}{r_M c_M}}.$$

Thus, if a cable has a constant radius R_0, the voltage in cable depends on neither the curvature nor the torsion. Furthermore, in this case voltage does not differ from the voltage for the straight cylindrical cable with the same radius.

Figure 2 shows the cable equation solution for a cylindrical cable.

In the following sections we will study cables with a variable radius.

V. AN EXACT SOLUTION WITH A VARIABLE RADIUS

Cables with a nonconstant radius are important for different reasons. For example, discrete swellings along the axons appear in neurodegenerative diseases such as Alzheimers, Parkinsons, HIV-associated dementia, and multiple sclerosis. In particular, in Parkinsons disease, there are reported axons with a diameter of approximately 1 μm with a swelling with diameter of approximately 5 μm, see Ref. [22]. In addition, in multiple sclerosis, there are reported axons with a diameter of approximately 4 μm with a swelling with a diameter of approximately 60 μm, see Ref. [23]. In Alzheimers disease there are reported axons with a diameter of approximately

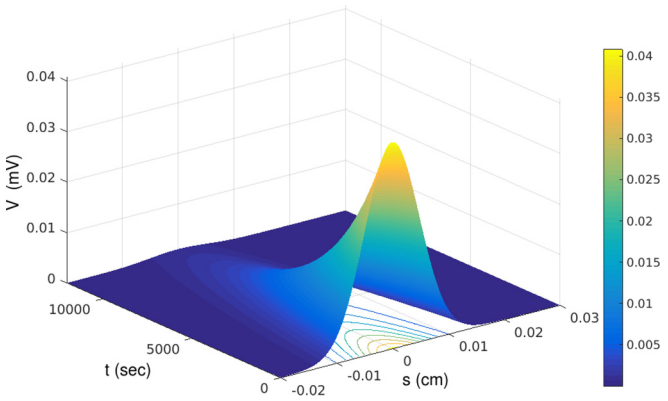

FIG. 2. Voltage for the cylindric cable. Parameter values used for simulations correspond to realistic dendritic parameters as in Ref. [14]: $c_M = 1$ mF/cm^2, $r_M = 3000\ \Omega\,\text{cm}^2$, $r_L = 100\ \Omega\,\text{cm}$, $R_0 = 10^{-4}$ cm. The initial condition is given by (47).

1.5 μm with a swelling train, where the swelling diameter varies between 4 μm and 10 μm, see Refs. [24–26]. For HIV-associated dementia, there are reported axons with a diameter of approximately 6 μm and swellings with a diameter of approximately 43 μm, see Refs. [27–31]. Other sizes of the axonal swellings can be see in Refs. [7,32].

When the radius $R(\theta,s)$ is not a constant, Eq. (34) is very complicated. However, some ideal cases can help us to understand the general case. In this section, we study an ideal case which does not represent a realistic axon or dendrite, but it will help us to understand the generalized cable equation (30).

If the cable curvature vanishes and the radius is

$$R(s) = R_0 \cosh\left(\frac{s}{R_0}\right), \tag{38}$$

then Eq. (34) becomes

$$\frac{\partial V(s,t)}{\partial t} = \frac{R_0}{2r_L c_M}\frac{\partial^2 V(s,t)}{\partial s^2} + \frac{1}{r_L c_M}\frac{\sinh\left(\frac{s}{R_0}\right)}{\cosh\left(\frac{s}{R_0}\right)}\frac{\partial V(s,t)}{\partial s} - \frac{V(s,t)}{r_M c_M},$$

which is solved by the voltage

$$V(s,t) = \frac{V_0 l_0^2}{R(s)}\sqrt{\frac{r_L c_M}{2\pi R_0 t}}\, e^{-\frac{r_L c_M s^2}{2R_0 t}}\, e^{-t\left(\frac{1}{r_M c_M}+\frac{1}{R_0 r_L c_M}\right)}. \tag{39}$$

Notice that when the radius (38) increases, the voltage (39) decreases.

In Fig. 3 we can see the voltage (39).

VI. GENERAL PROPERTIES

Studying the ideal cable (38) we learned that when the time increases the voltage (39) decreases. In addition, this voltage depends on $R^{-1}(s)$, namely this voltage depends on $[\sqrt{a(s)}]^{-1}$, where $a(s)$ is the cable cross-sectional area. Then, inspired in the ideal case (39), in order to study Eq. (30), we propose the following voltage

$$V(s,t) = \frac{\Psi(s,t)}{\sqrt{a(s)}}. \tag{40}$$

Thus, Eq. (30) implies

$$\frac{\partial \Psi(s,t)}{\partial t} = D(s)\frac{\partial^2 \Psi(s,t)}{\partial s^2} + \rho(s,t), \tag{41}$$

where

$$D(s) = \frac{a(s)}{r_L c_M \int_0^{2\pi} d\theta \sqrt{\det g(\theta,s)}},$$

$$\rho(s,t) = \frac{\sqrt{a(s)}}{r_L c_M \int_0^{2\pi} d\theta \sqrt{\det g(\theta,s)}}\left\{\frac{1}{4}\left[\frac{da(s)}{ds}\right]^2\frac{1}{a^{\frac{3}{2}}} - \frac{1}{2a^{\frac{1}{2}}(s)}\frac{d^2a(s)}{ds^2} - \frac{r_L\int_0^{2\pi} d\theta\sqrt{\det g(\theta,s)}}{r_M\sqrt{a(s)}}\right\}\Psi(s,t).$$

Notice that Eq. (41) can be interpreted as a diffusion equation with a source, in this equation the coefficient diffusion and the source term are generated by the cable geometry.

Now, we can see that if we take

$$\Psi(s,t) = e^{-Et}\psi(s), \tag{42}$$

where E is a constant with (time)$^{-1}$ dimensions, Eq. (41) becomes

$$-\frac{\partial^2 \psi(s)}{\partial s^2} + U(s)\psi(s) = 0, \tag{43}$$

where

$$U(s) = -\frac{\left[\frac{da(s)}{ds}\right]^2}{4a^2(s)} + \frac{1}{2}\frac{\frac{d^2a(s)}{ds^2}}{a(s)} - \frac{r_L c_M\left(E - \frac{1}{r_M c_M}\right)\int_0^{2\pi} d\theta\sqrt{\det g(\theta,s)}}{a(s)}. \tag{44}$$

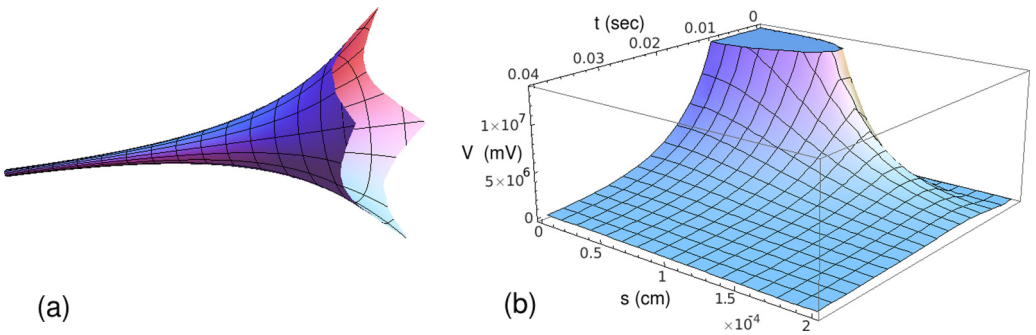

FIG. 3. (a) Cable with radius variable (38). (b) Voltage (39). Parameter values used for simulations correspond to realistic dendritic parameters as in Ref. [14]: $c_M = 1$ mF/cm^2, $r_M = 3000\ \Omega\,\text{cm}^2$, $r_L = 100\ \Omega\,\text{cm}$, $R_0 = 10^{-4}$ cm, $V_0 = 1$ mV, $l_0 = 1$ cm.

If $E = 0$, then Eq. (43) is the equilibrium description of the diffusion equation (41). Moreover, in some cases the Fokker-Planck equation and the diffusion equation can be rewritten as a Schrödinger equation [33]. In this respect, notice that Eq. (43) can be seen as a Schrödinger equation where $U(s)$ is an effective potential, which is generated by the cable geometry.

In particular, when the radius of the cable is a constant the effective potential is the constant

$$U(s) = U_0 = -\frac{2r_L c_M}{R_0}\left(E - \frac{1}{r_M c_M}\right). \tag{45}$$

When the radius is not a constant, the function $\psi(s)$ is affected by the effective potential (44). For example, if the cable has a circular cross section with radius $R(s)$, then the effective potential is

$$U(s) = \frac{1}{R(s)}\left\{\frac{1}{2}\frac{d^2R(s)}{ds^2} - \left(E - \frac{1}{r_M c_M}\right)\frac{r_L c_M}{\pi} \times \int_0^{2\pi} d\theta \sqrt{(1-\kappa(s)R(s)\cos\theta)^2 + \left[\frac{dR(s)}{ds}\right]^2}\right\}. \tag{46}$$

From this last equation we can see that if the derivatives of the radius $R(s)$ are small quantities, then the radius can be approximated by a constant and the effective potential can be approximated by a constant, too. In this case, the voltage in the cable is similar to the cylindrical cable. Moreover, observe that the condition (16) implies that $[1-\kappa(s)R(s)\cos\theta]^2$ is a small quantity. Then, when $(\frac{dR}{ds})^2$ is a large quantity and $[1-\kappa(s)R(s)\cos\theta]^2 \ll (\frac{dR}{ds})^2$, the effective potential (46) depends on neither the curvature nor the torsion. Thus, in this last case, cables with similar swelling have a similar voltage.

When the cable has a deformed circular cross section with radius $R = R(\theta,s)$, we should introduce Eqs. (32) and (33) into the effective potential (44). In this case we can see that the effective potential is affected by derivatives of the radius respect to the angle θ. Then, geometrical inhomogeneities on a cable might be affect the voltage.

In the next section we will provide numerical solution for cable with different geometries.

VII. NUMERICAL SOLUTIONS

In this section the differential equation (30) is solved by using the second-order finite-differences method for both spatial coordinate and temporal evolution. The choice of mesh size was made with the usual procedure. First, we begin with 1024 points along the s axis and 50 points in the time. The meshes for the s direction and for the time were refined several times. We stop when no differences in solutions are obtained in two successive refinements. The numbers of spatial and temporal points used in the simulation are shown in Table I.

The system is solved using the Gauss-Seidel iterative method, with a tolerance of 10^{-10}. Moreover, for the initial condition we used a Gaussian shape,

TABLE I. Numbers of points, n_s and n_t, and number of times of the refinement.

Refinement	n_s	n_t
First time	1024	50
Second time	2048	80
Third time	4096	100

$$V(s,0) = \frac{A}{\sqrt{2\pi\sigma}} e^{-\frac{s^2}{2\sigma^2}}, \tag{47}$$

where $A = 0.05\ \text{mV cm}^{\frac{1}{2}}$ and $\sigma = 100\ \Delta\text{s}$. In addition, we impose the Neumann boundary conditions [3]

$$\frac{\partial V(s_0,t)}{\partial s} = \frac{\partial V(s_{n_s},t)}{\partial s} = 0.$$

A. Cable with sinusoidal swelling

Now we study a cable with curvature $\kappa = 0$ and with the radius

$$R(s) = R_0(1 + \alpha_1 \sin\alpha_2 s). \tag{48}$$

In Fig. 4(a) we can see a cable with this geometry. Notice that in this case we should take $\alpha_1 < 1$. Furthermore, in order to obtain a realistic cable geometry, we should take $\alpha_2 < 1\ \text{cm}^{-1}$. Then, in this case, the derivatives of radius of the cable are small quantities. In fact, for this cable the effective potential is

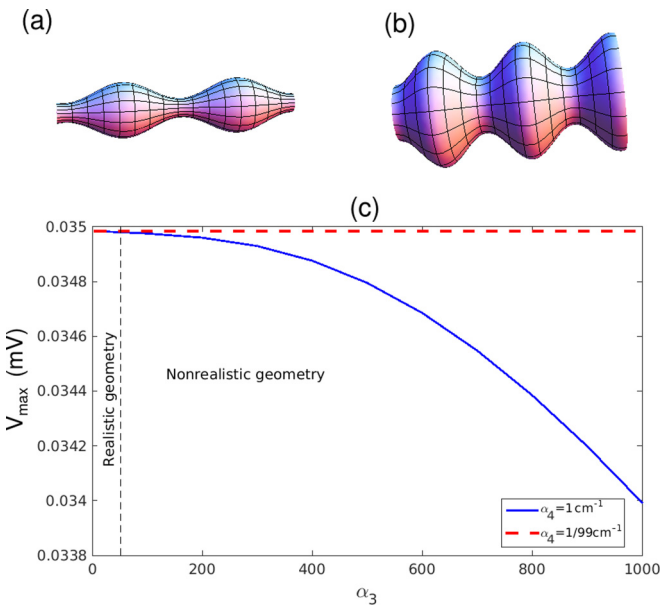

FIG. 4. (a) Cable with geometry (48). (b) Cable with geometry (50). (c) Maximum voltage for a cable with radius (50) at time $t = 1000$ s vs the parameter α_3. The voltage changes only if $\alpha_3 > 50$, a values for nonrealistic cable geometries with swellings. Parameter values used for simulations correspond to realistic dendritic parameters as in Ref. [14]: $c_M = 1\ \text{mF/cm}^2$, $r_M = 3000\ \Omega\,\text{cm}^2$, $r_L = 100\ \Omega\,\text{cm}$, $R_0 = 10^{-4}$ cm. The initial condition is given by (47).

given by

$$U(s) = -\frac{1}{1+\alpha_1 \sin\alpha_2 s}\left(\frac{1}{2}\alpha_1\alpha_2^2 \sin\alpha_2 s + \frac{2}{R_0}\left(E - \frac{1}{r_M c_M}\right) r_L c_M \sqrt{1 + R_0^2\alpha_1^2\alpha_2^2 \cos^2\alpha_2 s}\right). \tag{49}$$

Notice that for realistic cable geometry the inequality $\alpha_1\alpha_2 \ll 1\ \mathrm{cm}^{-1}$ is satisfied and the effective potential is a small quantity. Then, in this case, the voltage in the cable is similar to voltage in the cylindrical cable.

A similar result is obtained when the radius of the cable is given by

$$R(s) = R_0(1 + \alpha_3 \sin^2\alpha_4 s). \tag{50}$$

In Fig. 4(b) we can see a cable with this geometry.

Notice that in this case α_3 can be bigger than 1, and for a realistic cable geometry the condition $\alpha_3\alpha_4 \ll 1\ \mathrm{cm}^{-1}$ should be satisfied. It can be shown that in this case the effective potential (46) is a small quantity and then the voltage in the cable also does not diffe from the voltage for the cylindrical cable.

In Fig. 4(c), we plot the maximum voltage as a function of α_3 for two different values of α_4. We can see that the voltage to cable with a realistic geometry does not differ from the voltage for a cylindrical cable.

B. Cable with Gaussian swelling

Now, we study a cable with the radius

$$R(s) = R_0[1 + \alpha_3 e^{-\alpha_5(s-\alpha_6)^2}]. \tag{51}$$

In Fig. 5(a) can see a cable with this geometry. The numerical solution to the voltage can be seen in Fig. 5(b). In this figure we can see that the voltage decreases faster than the voltage to the cylindrical cable. Notice that for this geometry when the height of the swelling (51) increases the voltage of the cable decreases. In fact, for a big α_3 parameter the voltage can be blocked.

C. Cable with Gaussian swellings

In this section we study the cable with the following radius:

$$R(s) = R_0[1 + \alpha_3 e^{-\alpha_5 s^2} + \alpha_3 e^{-\alpha_5(s-\alpha_6)^2} + \alpha_3 e^{-\alpha_5(s-2\alpha_6)^2} + \alpha_3 e^{-\alpha_5(s-3\alpha_6)^2}]. \tag{52}$$

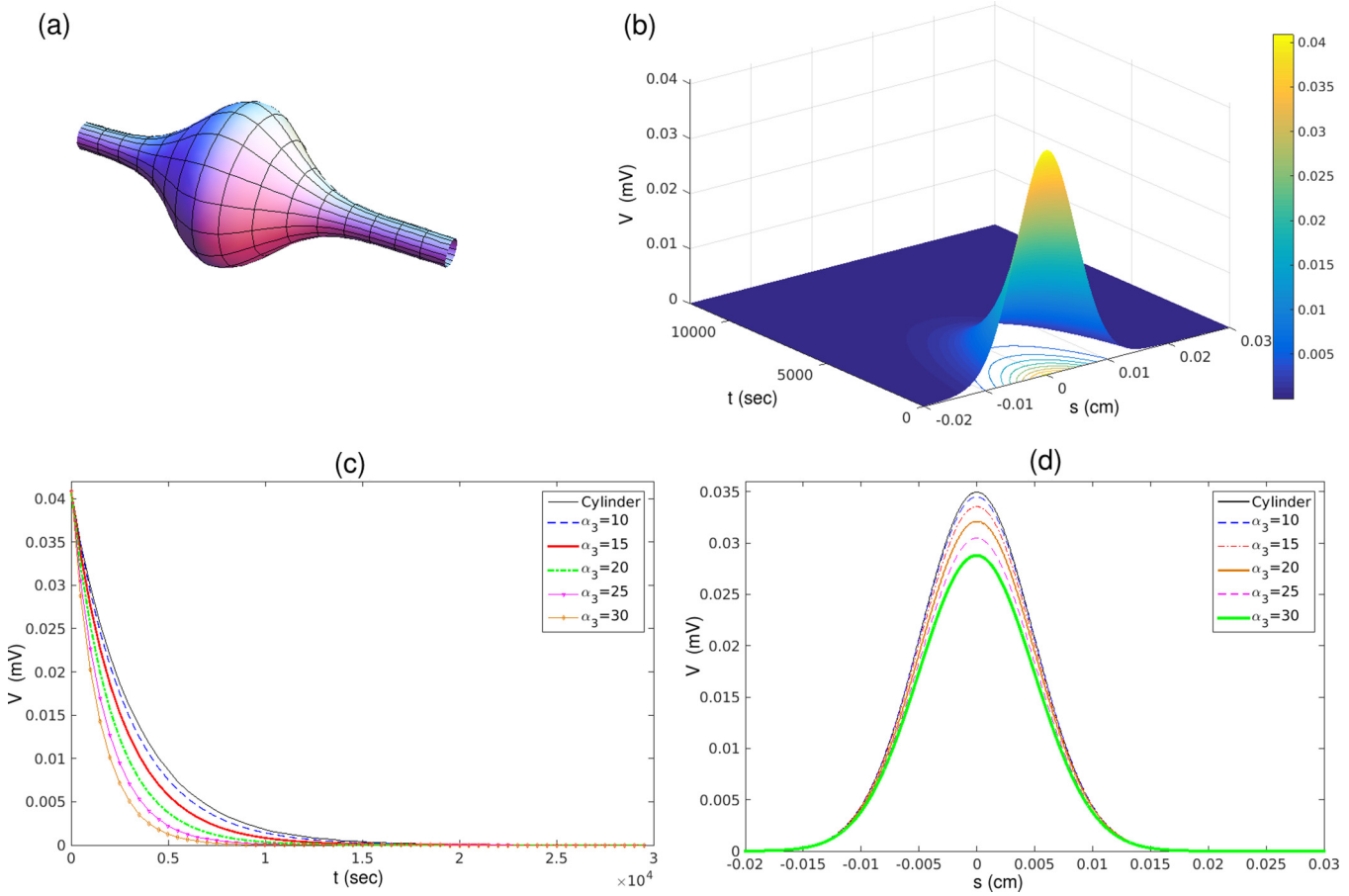

FIG. 5. (a) Cable with geometry (51). (b) Voltage for the cable with a Gaussian swelling, radius (51). (c) Voltage vs t in $s = 0$ with different values for α_3. (d) Voltage vs s at time $t = 1000$ s for different values of α_3. Parameter values used for simulations correspond to realistic dendritic parameters as in Ref. [14]: $c_M = 1\ \mathrm{mF/cm^2}$, $r_M = 3000\ \Omega\,\mathrm{cm^2}$, $r_L = 100\ \Omega\,\mathrm{cm}$, $R_0 = 10^{-4}$ cm. The initial condition is given by (47).

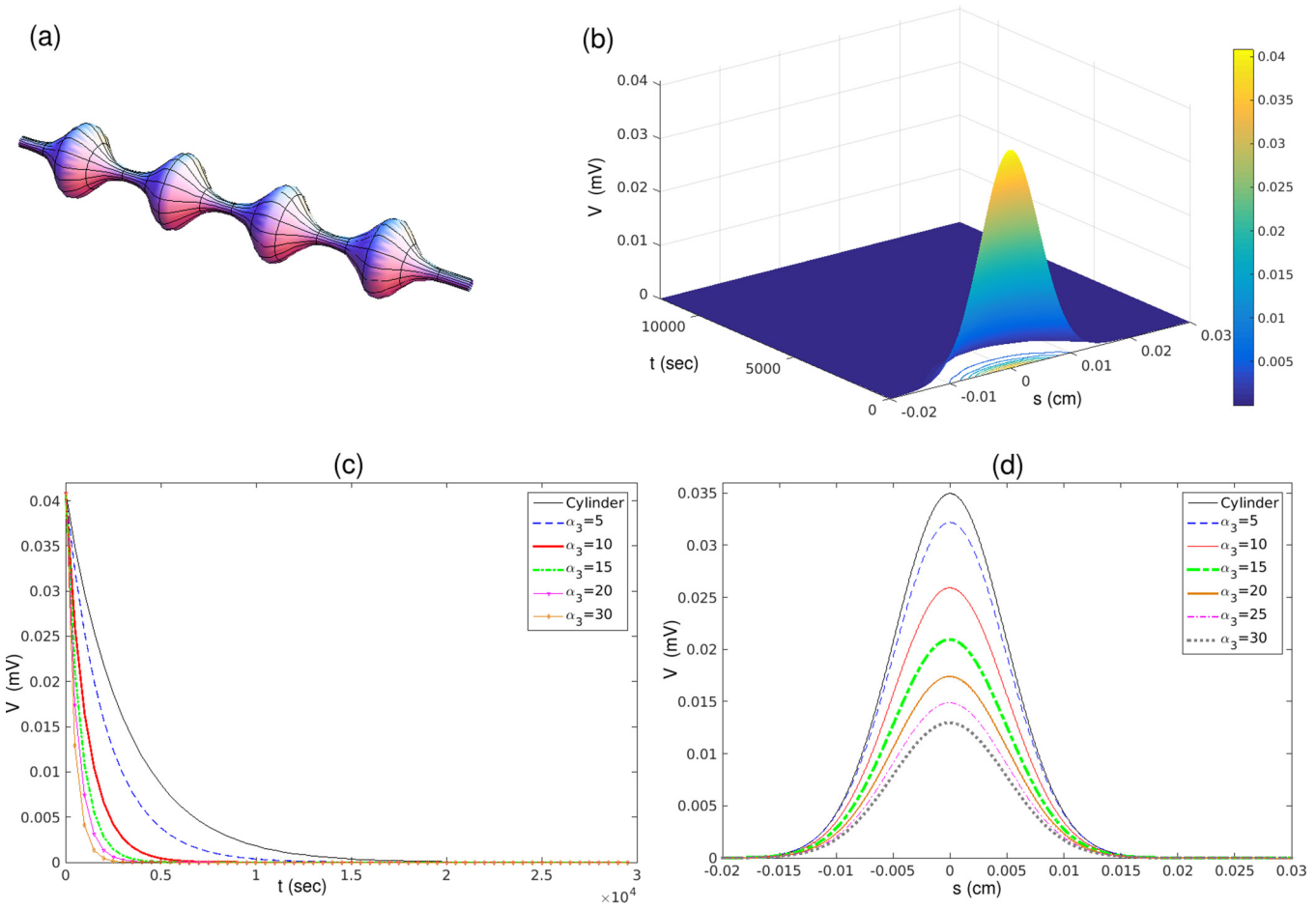

FIG. 6. (a) Cable with geometry (52). (b) Voltage for the cable with a Gaussian train swellings, radius (52). (c) Voltage vs t in $s = 0$ with different values for α_3. (d) Voltage vs s at time $t = 1000$ s for different values of α_3. Parameter values used for simulations correspond to realistic dendritic parameters as in Ref. [14]: $c_M = 1$ mF/cm^2, $r_M = 3000\ \Omega\,\text{cm}^2$, $r_L = 100\ \Omega\,\text{cm}$, $R_0 = 10^{-4}$ cm. The initial condition is given by (47).

A cable with this geometry can be seen in Fig. 6(a) and the numerical solution to the voltage in this cable can be seen in Fig. 6(b). In this case we can see that the voltage decreases faster than the voltage to the cylindrical cable. Moreover, notice that for this geometry when the height of the swelling (52) increases the voltage of the cable decreases. Observe that the voltage in this cable decreases more than the voltage in the cable with radius (51). Actually, if α_3 is a big parameter, then the voltage can be blocked.

D. Amorphous swelling

In the literature there are reported axons with amorphous swelling [6]. For an amorphous cable we can propose the following radius:

$$R(\theta,s) = R_0[1 + \alpha_3 e^{-\alpha_5(s-\alpha_6)^2} + \alpha_7 \sin\theta\cos\alpha_8 s]. \quad (53)$$

A cable with this geometry can be seen in Fig. 7(a) and the numerical solution for the voltage in this cable can be seen in Figs. 7(b)–7(d). In this case we can see that the voltage decreases faster than the voltage to the cylindrical cable. In addition, observe that the voltage in this cable decreases more than the voltage in the cable with radius (51). Thus, geometric inhomogeneities in a cable can change its voltage in it.

Axons with swellings are hallmark features of some neurodegenerative diseases such as Alzheimers, Parkinsons, HIV-associated dementia, and multiple sclerosis [6–8]. The numerical results of this section indicate that when the cable geometry is important to the voltage propagation. These results show that when the derivatives of the cable radius are slowly changing functions, namely when $(\frac{dR}{ds})^2 \ll [1 - \kappa(s)R(s)\cos\theta]^2$ and $\frac{d^2R(s)}{ds^2} \ll \frac{r_L}{r_M}$, the voltage is similar to voltage in a straight cylindrical cable. However, when these derivatives change significantly the voltage cable is reduced and, in a extreme case, it can be blocked. Moreover, these numerical results show that geometric inhomogeneities in a cable can affect the voltage.

VIII. SUMMARY

In this paper, using the Frenet-Serret frame, we proposed a cable with general geometry and construct a generalized cable equation to the voltage in it. This generalized equation depends on geometric quantities as curvature and torsion of the cable. For the general case, this equation is very complicated to obtain exact solutions. However, when the cable has a constant

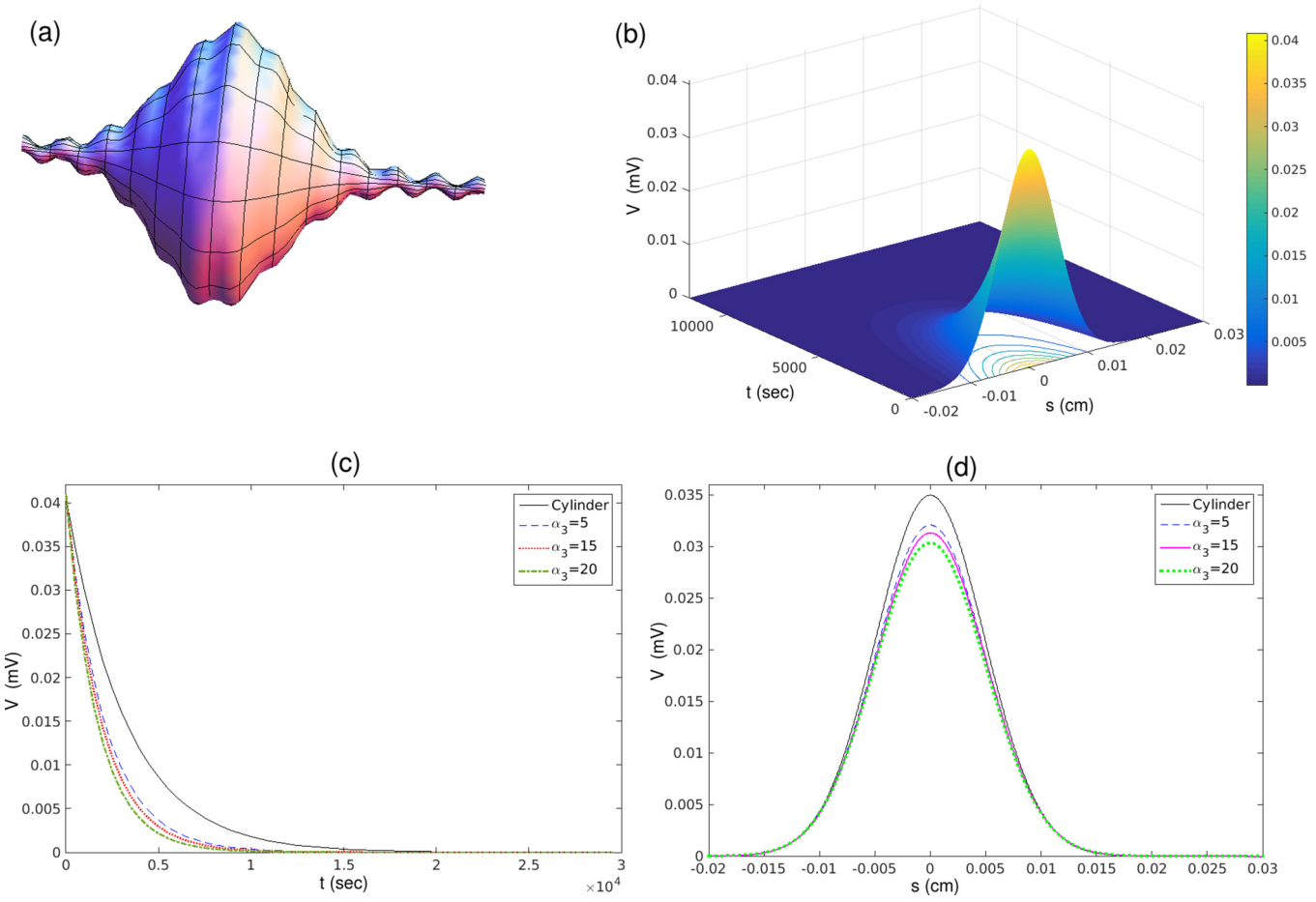

FIG. 7. (a) Cable with geometry (53). (b) Voltage for the cable with the radius (53). (c) Voltage vs t in $s = 0$ with different values for α_3. (d) Voltage vs s at time $t = 1000$ s for different values of α_3. Parameter values used for simulations correspond to realistic dendritic parameters as in Ref. [14]: $c_M = 1$ mF/cm^2, $r_M = 3000\ \Omega\,\text{cm}^2$, $r_L = 100\ \Omega\,\text{cm}$, $R_0 = 10^{-4}$ cm. The initial condition is given by (47).

circular cross section, we showed that the equation depends on neither the curvature nor the torsion of the cable. In fact, in this last case the new equation is equivalent to the cable equation for a straight cylindrical cable, where the voltage depends on the arc length parameter. This shows that the natural variables for the voltage are given by the cable geometric quantities. Additionally, we found an exact solution for an ideal cable with a particular nonconstant circular cross section and zero curvature. In this last case, we show that when the radius increases, the voltage decreases. Inspired in this ideal case, we rewrote the generalized cable equation as a diffusion equation with a source term. In this diffusion equation the source term and the diffusion coefficient are generated by the cable geometry. Furthermore, we provided numerical solutions to the new cable equation to different cable with swelling. These solutions show that when the derivatives of the cable radius are slowly changing functions the voltage is similar to voltage in a straight cylindrical cable. However, when these derivatives change significantly the voltage cable is reduced and, in a extreme case, it can be blocked. Moreover, these numerical results show that geometric inhomogeneities in a cable can change its voltage in it. The results of this paper might help us to understand the behavior of the voltage in focal axonal swellings which appear in some neurodegenerative diseases such as Alzheimers, Parkinsons, HIV-associated dementia, and multiple sclerosis [6].

In this work we did not study the active case, but we can argue that when the cable has a constant circular cross section the active case does not differ from the usual active cylindrical cable. In a future work we will study the active cable case and some important cable geometries, for instance, the spiny cable geometry.

ACKNOWLEDGMENTS

This work was supported in part by CONACyT-SEP CB 2012-180111-F (J.M.R.). We are grateful to the referees for providing valuable comments.

[1] W. Rall, Cable theory for dendritic neurons, in *Methods in Neuronal Modeling: From Synapses to Networks*, edited by C. Koch and I. Segev (MIT Press, Cambridge, MA, 1989), Chap. 2.

[2] W. Rall, Theoretical significance of dendritic trees for neuronal input-output relations, in *Neural Theory and Modeling*, edited by R. F. Reiss (Sanford University Press, Stanford, CA, 1964), p. 73.

[3] G. B. Ermentrout and D. H. Terman, *Mathematical Foundation of Neuroscience* (Springer, London, 2010).
[4] P. C. Bressloff, *Waves in Neural Media: From Single Neurons to Neural Fields* (Springer, London, 2014).
[5] Q. Caudron, S. R. Donnelly, S. P. C. Brand, and Y. Timofeeva, Computational convergence of the path integral for real dendritic morphologies, J. Math. Neurosci. **2**, 11 (2012).
[6] P. D. Maia, M. A. Hemphill, B. Zehnder, C. Zhang, K. K. Parker, and J. N. Kutz, Diagnostic tools for evaluating the impact of Focal Axonal Swellings arising in neurodegenerative diseases and/or traumatic brain injury, J. Neurosci. Methods **253**, 233 (2015).
[7] M. H. Magdesian, F. S. Sanchez, M. Lopez, P. Thostrup, N. Durisic, W. Belkaid, D. Liazoghli, P. Grütter, and D. R. Colman, Atomic force microscopy reveals important differences in axonal resistance to injury, Biophys. J. **103**, 405 (2012).
[8] T. C. Yin, J. R. Voorhees, R. M. Genova, K. C. Davis, A. M. Madison, J. K. Britt, C. J. Cintrón-Pérez, L. McDaniel, M. M. Harper, and A. A. Pieper, Acute axonal degeneration drives development of cognitive, motor, and visual deficits after blast-mediated traumatic brain injury in mice, eNeuron **3**, e0220-16 (2016).
[9] P. Vetter, A. Roth, and M. Hausser, Propagation of action potentials in dendrites depends on dendritic morphology, Neurophysiol **85**, 926 (2001).
[10] A. D. Bird and H. Cuntz, Optimal current transfer in dendrites, PLoS Comput Biol. **12**, e1004897 (2016).
[11] F. Santamaria, S. Wils, E. De Schutter, and G. J. Augustine, Anomalous diffusion in purkinje cell dendrites caused by spines, Neuron **52**, 635 (2006).
[12] E. R. Kandel, J. H. Schwartz, and T. N. Jessell, *Principles of Neural Science* (McGraw-Hill, New York, 2000).
[13] J. C. Fiala and K. M. Harris, Dendrite structure, in *Dendrites*, edited by G. Stuart, N. Spruston, and M. Häusser (Oxford University Press, Oxford, 1999), p. 1.
[14] R. R. Poznanski, Modelling the electrotonic structure of starburst amacrine cells in the rabbit retina: A functional interpretation of dendritic morphology, Bull. Math. Biol. **54**, 905 (1992).
[15] H. Anwar, C. J. Roome, H. Nedelescu, W. Chen, B. Kuhn, and E. De Schutter, Dendritic diameters affect the spatial variability of intracellular calcium dynamics in computer models, Front. Cell. Neurosci. **8**, 168 (2014).
[16] K. A. Lindsay, J. R. Rosenberg, and G. Tucker, From Maxwell's equations to the cable equation and beyond, Progr. Biophys. Molec. Biol. **85**, 71 (2004).
[17] C. Bedárd and A. Destexhe, Generalized cable theory for neurons in complex and heterogeneous media, Phys. Rev. E **88**, 022709 (2013).
[18] C. Bedárd and A. Destexhe, Generalized cable formalism to calculate the magnetic field of single neurons and neuronal populations, Phys. Rev. E **90**, 042723 (2014)
[19] M. P. Do Carmo, *Differential Geometry of Curves and Surfaces* (Dover, New York, 2016).
[20] M. Spivak, *A Comprehensive Introduction to Differential Geometry*, Vol. II (Publish or Perish, Houston 1975).
[21] W. Greiner, *Classical Electrodynamics* (Springer-Verlag, New York, 1991).
[22] J. E. Galvin, K. Uryu, V. M.-Y. Lee, and J. Q. Trojanowski, Axon pathology in Parkinson's disease and Lewy body dementia hippocampus contains α-, β-, and γ-synuclein, Proc. Natl. Acad. Sci. USA **96**, 13450 (1999).
[23] B. D. Trapp, J. Peterson, R. M. Ransohoff, R. Rudick, S. Mörk, and L. Bö, Axonal transection in the lesions of multiple sclerosis, New Engl. J. Med. **338**, 278 (1998).
[24] V. E. Johnson, W. Stewart, and D. H. Smith, Axonal pathology in traumatic brain injury, Exp. Neurol. **246**, 35 (2013).
[25] D. Krstic and I. Knuesel, Deciphering the mechanism underlying late-onset Alzheimer disease, Nat. Rev. Neurosci. **9**, 25 (2013).
[26] H. Xie, J. Guan, L. A. Borrelli, J. Xu, A. Serrano-Pozo, and B. J. Bacskai, Mitochondrial alterations near amyloid plaques in an Alzheimer's disease mouse model, J. Neurosci. **33**, 17042 (2013).
[27] H. Budka, G. Costanzi, S. Cristina, A. Leehi, C. Parravicini, R. Trabattoni, and L. Vago, Brain pathology induced by infection with the human immunodeficiency virus (HIV), Acta Neuropathol. **75**, 185 (1987).
[28] F. Gray, F. Chrétien, A. V. Vallat-Decouvelaere, and F. Scaravilli, The changing pattern of HIV neuropathology in the HAART era, J. Neuropathol. Exp. Neurol. **62**, 429 (2003).
[29] M. Kaul, G. A. Garden, and S. A. Lipton, Pathways to neuronal injury and apoptosis in HIV-associated dementia, Nature **410**, 988 (2001).
[30] F. Raja, F. E. Sherriff, C. S. Morris, L. R. Bridges, and M. M. Esiri, Cerebral white matter damage in HIV infection demonstrated using β-amyloid precursor protein immunoreactivity, Acta Neuropathol. **93**, 184 (1997).
[31] R. Ellis, D. Langford, and E. Masliah, HIV and antiretroviral therapy in therain: Neuronal injury and repair, Nat. Rev. Neurosci. **8**, 33 (2007).
[32] G. M. G. Shepherd and K. M. Harris, Three-dimensional structure and composition of CA3 $\rightarrow$ CA1 axons in rat hippocampal slices: Implications for presynaptic connectivity and compartmentalization, J. Neurosci. **18**, 8300 (1980).
[33] H. Risken, *The Fokker-Planck Equation, Methods of Solution and Applications* (Springer-Verlag, New York, 1989).